ANNAL OF GEOPHYSICS, 67, 1, PA107, 2024; doi:10.4401/ag-9031
OPEN ACCESS

Can seismogenic atmospheric current influence the ionosphere?

Vadim V. Surkov and Vyachelsav A. Pilipenko*

Institute of Physics of the Earth, Russian Academy of Sciences, B. Gruzinskaya 10, Moscow 123242, Russia

Article history: received October 30, 2023; accepted March 5, 2024

Abstract

The question of whether earthquake precursors can arise in the ionosphere is of a special interest in geophysics. Despite numerous encouraging reports on seismo-ionospheric effects, the mechanism of the lithosphere-atmosphere-ionosphere coupling (LAIC) during the crust destruction phase was not revealed yet. One of hypothesis assumes that a seismogenic current transfers an abnormal electric field from the near-surface atmosphere to the ionosphere prior to an earthquake occurrence. This current can be caused by the air ionization due to enhancement of radon gas emission from the soil or upward movement of charged atmospheric aerosols. Here we present a theoretical model of the spatial structure of the electric field in the atmosphere and bottom ionosphere driven by a vertical extrinsic current in the lower atmosphere. Perturbation of electric field in the ionosphere has been derived in the approximation of the "thin" E-layer. Simple analytical estimates have been obtained that relate the horizontal electric field in the ionosphere, vertical electric field on the ground, and parameters of the external current. The electric field attenuation with altitude is caused by the increase of atmospheric conductivity and the horizontal spreading of current. The estimates obtained enable one to evaluate the feasibility of anomalous variations of electric fields in the ionosphere related to forthcoming earthquakes. The analysis has shown that the hypothesis on aerosol upward convection as a cause of ionospheric anomalies seems unrealistic. To interpret the occurrence of significant ionospheric anomalies it would be necessary to assume the presence of too large currents and electric fields in the lower atmosphere that had never been observed during non-thunderstorm periods.

Keywords: Ionospheric earthquake precursor; Aerosols; Radon emission; Seismogenic current; Atmospheric electric field

1. Introduction

Energy accumulation and redistribution before a seismic shock is a large-scale global phenomenon, involving all geospheres. The outer geoshell – ionosphere, is a thin layer of ionized plasma which is highly sensitive to any impact not only from above, but from below as well [Popov et al. 1989]. Geophysical community hopes to apply the ionosphere monitoring by ground or satellite technique for operative detection of seismic related precursors before severe earthquakes [Pulinets and Boyarchuk 2004]. However, numerous reports on possible

seismo-ionospheric anomalies made with the vertical ionosonde sounding [Korsunova and Khegai 2018], radiowave probing of the ionosphere – ground waveguide [Rozhnoi et al. 2006], monitoring the integral total electron content (TEC) of the ionospheric plasma with the use of global navigation satellite systems [Liu et al. 2004; Le et al. 2013; Kelley et al. 2017] still remain empirical. The actual mechanism of the lithosphere – atmosphere – ionosphere coupling (LAIC) has not been identified yet. This situation causes doubt on statistical significance of the reported relationships between ionospheric variations and earthquakes [Dautermann et al. 2007; Kamogawa and Kakinami 2013; Thomas et al. 2017; Masci et al. 2017].

Several possible channels of LAIC were suggested so far. It was assumed that this coupling can occur through the acoustic channel performed by acoustic-gravity waves (AGWs) [Gokhberg and Shalimov 2000; Pulinets and Ouzounov 2011; Klimenko et al. 2011] although the generation mechanism of AGWs by a pre-earthquake activity is not clear. While the AGW energy generated during earthquake shock and tsunamis is known to be sufficient to cause the ionospheric response [Astafyeva et al. 2014; Jin et al. 2015; Shalimov et al. 2019; Sorokin et al. 2019], the generation of AGWs by some pre-earthquake activity is still difficult to explain [Hayakawa et al. 2007].

Atmospheric electric field E_z, much greater than the fair-weather field of ~100 V/m, was observed near the ground a few days before earthquakes [Rulenko et al. 1992; Rulenko 2000; Hao et al. 2000]. It was hypothesized that the intense atmospheric electric fields may be responsible for the electrostatic channel of LAIC [Pulinets et al. 2000]. Disturbed quasi-DC electric field in the upper ionosphere above epicenters of forthcoming earthquakes was found even by low-Earth orbit (LEO) satellites. LEO observations above upcoming earthquake epicenters revealed the electric field bursts up to 2-10 mV/m [Chmyrev et al.1989; Gousheva et al. 2009]. Electric field anomalies ~1 mV/m above the earthquake epicenter were detected by FORMOSAT-5 satellite 7 days before $M = 6.8$ earthquake [Liu and Chao 2017]. The computer simulations showed that the observable TEC perturbation due to a vertical plasma drift requires an additional zonal electric field in the F-layer with an amplitude of 3-9 mV/m [Zolotov et al. 2012; Klimenko et al. 2011].

In the numerical simulations, the origin of the seismogenic current and the nature of the nonelectrostatic forces driving this current are not specified. Instead, the distribution of the vertical electric field $\mathbf{E}$ is set on the earth's surface [Kim et al. 2002, 2012, 2017; Hegai et al. 2015; Khegai 2020]. And then a stationary problem is solved for the electric field and conduction currents in the atmosphere and ionosphere. Note that this approach differs from the standard one, when zero electric potential is set on the surface of an ideally conducting earth. In fact, this approach means that the density of the conduction current $\mathbf{j} = \sigma\mathbf{E}$ is set on the earth's surface, which flows from the earth's surface into the atmosphere. Based on this model Kim et al. [2017], Hegai et al. [2015], and Khegai [2020] claimed that a large-scale electric field $E_z > 1$ kV/m is needed to cause the electric field disturbance in the nightside ionosphere of a few mV/m.

Theoretical investigations of similar topics were done by Park and Dejnakarintra [1973] who studied the ionospheric response to charged thunderstorm clouds. Very roughly, all the models predicted that the large-scale DC electric field attenuation is about the ratio of conductivities near the ground and at the bottom ionosphere (~80 km), $\sim 10^{-6}$. However, the simulation in [Denisenko et al. 2013] showed that an atmospheric electric field with amplitude 100 V/m could provide the electric fields in the ionosphere just ≤1 μV/m during night-time. The ionospheric response during daytime was estimated to be 1-2 orders less than during night-time, because the electric field penetration was inversely proportional to the ionospheric conductance. The ionospheric E-field response decreased if the horizontal size of the earthquake preparatory zone became smaller than 400 km, and dropped severely for the scales ≪ 100 km. Thus, the feasibility of the electrostatic channel of LAIC is still ambiguous.

The atmospheric current between the ground and the bottom ionosphere may be severely distorted by enhancement of radon gas emanation from soil, which occasionally occurred during seismic activity [Virk and Singh 1994; Yasuoka et al. 2009; Chowdhury et al. 2022]. However, some researchers did not find any statistically significant changes in the radon activity before earthquakes [e.g., Cigolini et al. 2015]. The increase of the air ionization due to the radioactive decay of radon nuclei results in an enhancement of the atmospheric electrical conductivity, which, in turn, modifies the fair-weather electric current [Harrison et al. 2010; Ouzounov et al. 2011; Pulinets and Davidenko 2014; Surkov 2015]. However, theoretical analysis showed that such electro-chemical channel of LAIC hardly can produce any noticeable variations of the electron density or electric field in the ionosphere [Sorokin and Hayakawa 2013; Surkov et al. 2023].

According to another hypothesis, electrical perturbations in the atmosphere are caused by currents in the earth, which are carried by so-called positive holes (p-holes) [Freund et al. 2021]. The rock conductivity due to

p-holes is assumed to prevail in the middle and partly in the lower crust under the influence of high stresses and deformations. It was hypothesized by Freund et al. [2021] that the p-holes move from the earthquake focal zone towards the less stressed regions, and then pile up in the thin surface layers of the Earth, thereby producing an upward-directed electric field in the atmosphere. This field is assumed to be so large that it can lead to the air ionization in the lower layers of the atmosphere. According to this hypothesis, the electric current in the atmosphere arises due to the drift of electrons and negatively charged particles from the atmosphere towards positively charged the earth surface. Thus, the seismogenic telluric current driven by non-electromagnetic forces is converted into a conduction current at the earth-atmosphere boundary. This model has been used to estimate the effect of the atmospheric current on the ionosphere [Kuo et al. 2011]. Numerical simulations show that a vertical current density of 0.2-10 μA/m^2 in rocks is necessary for the appearance of TEC variations, possibly related to impending earthquakes. The same current should occur in the atmosphere, due to the continuity of the vertical component of the current density at the earth-atmosphere boundary. This hypothesis is highly conjectural, since this current is five to seven orders of magnitude greater than the fair-weather atmospheric current (~1 pA/m^2).

The main features of other model by Kuo et al. [2014] is that the current density $\mathbf{j}$ is determined through a potential function ψ according to the relationship $\mathbf{j} = -\nabla\psi$. In that case, the function ψ may not be related to the potential of the electric field φ. Prokhorov and Zolotov [2017] have shown that above equation for $\mathbf{j}$ does not satisfy well-known set of the current continuity equation $\nabla \cdot \mathbf{j} = 0$ and usual Ohm's law $\mathbf{j} = -\hat{\sigma}\nabla\varphi$ except for the case when the electric conductivity tensor $\hat{\sigma}$ is a spatially invariant scalar. Whence it follows that this approach is not applicable to actual conditions, since the atmospheric conductivity strongly depends on altitude.

Finally, the suggestion was put forward that seismo-preparatory process may stimulate the upward flow of charged aerosols contained in the soil and near-surface atmospheric layer. Despite their insignificant percentage in the air in comparison to the other elements, aerosols play a significant role in the atmospheric thermal and electrical conditions [Namgaladze et al. 2018]. Aerosol particles capture the radioactive particles and transport radioactivity for a considerable distance from natural or anthropogenic sources. The aerosols alter the electrical conductivity of the air due to the attachment of light ions and free electrons. Moreover, the aerosols may be involved in the formation of the extraneous vertical electric current [Namgaladze and Karpov 2015]. These aerosols can be captured by upward convective and turbulent air movements, thereby producing vertical flow of charged aerosols, which in turn can transfer electric perturbations from the lower atmosphere to the lower ionosphere [Pulinets and Boyarchuk 2004; Klimenko et al. 2011; Sorokin and Hayakawa 2014]. Such "aerosol" channel was claimed to be more effective mechanism of LAIC [Pulinets et al. 1997; Kim et al. 2002; Sorokin and Ruzhin 2015]. The seismogenic current due to the turbulent upward diffusion of air with embedded charged aerosol particles was suggested to exceed significantly the fair-weather current and acts as an additional electromotive force (EMF) in the global electric circuit [Sorokin et al. 2007].

It is essential to understand how quasi-DC electric fields originating in the near-surface atmosphere by any mechanism penetrate to higher altitudes and into the ionosphere. The main purpose of our study is to analyze theoretically the plausibility of hypothesis about the impact of seismogenic vertical current on the ionosphere on the basis of a fairly general model which can be applied to a seismogenic/extrinsic current of any origin. We have elaborated the analytical model which provides the estimates of the electric fields in the ionosphere and on the ground for any parameters of seismogenic current. As compared with numerical models calculated for a fixed set of parameters, an analytical model has the advantage to describe explicitly the dependence of the effect on primary parameters.

2. Model of extrinsic current and basic equations

Let us assume that there is an extrinsic quasi-DC vertical current in the near-surface atmosphere, which results in perturbations of local electric field. In this section, we first examine the features of these perturbations, without specifying the physical nature of this extrinsic current. We consider a plane-stratified model of the medium, as illustrated in Figure 1, in which the atmosphere occupies a layer $0 < z < L$ between two conductive regions that mimic the ground ($z < 0$) and the ionosphere ($z > L$). The origin of the coordinate system is located on the ground surface ($z = 0$), while the positive z-axis is directed upward.

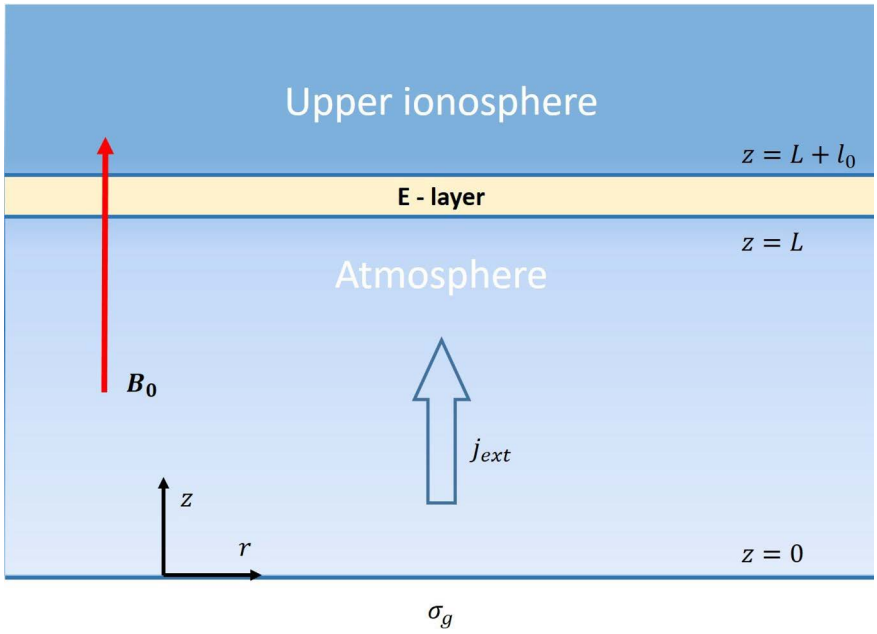

Figure 1. A sketch of the model geometry.

The ground is a semi-space with the homogeneous conductivity σ_g. The atmospheric conductivity $\sigma_a(z)$ increases exponentially with altitude as follows $\sigma_a(z) = \sigma_a \exp(z/l)$. In the ionosphere, that is above ~80 km, the conductivity of the ionospheric plasma becomes anisotropic. The Ohm's law for the perturbation of the current density in the ionosphere can be written as

$$\mathbf{j}_i = \sigma_\parallel \mathbf{E}_\parallel + \sigma_P \mathbf{E}_\perp + \sigma_H (\mathbf{B}_0 \times \mathbf{E}_\perp)/B_0, \tag{1}$$

where $\mathbf{B}_0$ is the geomagnetic field; $\mathbf{E}_\parallel$ and $\mathbf{E}_\perp$ denote the parallel and perpendicular components of the electric field with respect to $\mathbf{B}_0$; $\sigma_\parallel$ is the longitudinal (field-aligned) conductivity of the ionospheric plasma; σ_P and σ_H are the Pedersen and Hall conductivities, respectively. For simplicity, we assume that $\mathbf{B}_0$ is directed along the vertical z-axis. In such a case we come to an axisymmetric problem in which all the functions depend on two variables: the altitude z and polar radius r.

In the framework of this medium model, we consider the stationary problem of the distribution of electric fields and currents. In the atmosphere an axisymmetric extrinsic current with density $\mathbf{j}_{\text{ext}} = j_0(z)\exp(-r^2/r_0^2)\hat{\mathbf{z}}$, where r_0 is the characteristic transverse scale of the current, is directed along the z-axis. The function $j_0(z)$ may have different forms depending on the source of the current. The total atmospheric current $\mathbf{j}_a(r, z)$ is a sum of the conduction and extrinsic currents

$$\mathbf{j}_a(r, z) = \sigma_a(z)\mathbf{E} + j_0(z)\exp(-r^2/r_0^2)\hat{\mathbf{z}}, \tag{2}$$

where $\mathbf{E}$ stands for a perturbation of the electric field caused by the extrinsic current.

In the stationary case, the current density in all media must obey the continuity equation $\nabla \cdot \mathbf{j} = 0$. Additionally, the equation $\nabla \times \mathbf{E} = 0$ takes place, whence it follows that the electric field can be expressed from potential function φ through $\mathbf{E} = -\nabla\varphi$. Let us substitute Eq. (2) into the current continuity equation. Taking into account the azimuthal symmetry of the problem we write this equation in cylindrical coordinates r, z as follows

$$\frac{1}{r}\frac{\partial}{\partial r}(rE_r) + \frac{\partial E_z}{\partial z} + \frac{E_z}{\sigma_a}\frac{d\sigma_a}{dz} + \frac{1}{\sigma_a}\frac{dj_0}{dz}\exp\left(-\frac{r^2}{r_0^2}\right) = 0. \tag{3}$$

Substituting the dependence $\sigma_a(z)$ into Eq. (3) and expressing the radial E_r and vertical E_z components through the potential φ, we obtain

$$\hat{\Delta}_r\varphi + \frac{\partial^2\varphi}{\partial z^2} + \frac{1}{l}\frac{\partial\varphi}{\partial z} = \frac{1}{\sigma_0}\frac{dj_0}{dz}\exp\left(-\frac{r^2}{r_0^2} - \frac{z}{l}\right), \quad \hat{\Delta}_r = \frac{1}{r}\frac{\partial}{\partial r}r\frac{\partial}{\partial r}, \tag{4}$$

where $\hat{\Delta}_r$ denotes the radial part of the Laplace operator. Substitution of the current density in the homogeneous ground $\mathbf{j}_g = \sigma_g\mathbf{E}$ into the continuity equation yields

$$\hat{\Delta}_r\varphi + \frac{\partial^2\varphi}{\partial z^2} = 0. \tag{5}$$

Even though the ground conductivity does not enter Eq. (5), it affects the atmospheric field structure via the boundary condition. This condition states that the potential φ and normal component of the current density j_z must be continuous on the ground surface ($z = 0$).

Now we derive the boundary condition at the bottom edge of the ionosphere in the "thin" layer approximation. To do this we integrate the continuity equation $\nabla\cdot\mathbf{j} = 0$ along z from $z = L$ to $z = L + l_0$, where l_0 is the thickness of the conducting gyrotropic E-layer. Then making formally the transition $l_0 \to 0$ we obtain the following boundary condition at $z = L$:

$$[j_z] = \Sigma_P\hat{\Delta}_r\varphi, \quad \Sigma_P = \int_0^L \sigma_P(z')\,dz'. \tag{6}$$

Here the square brackets denote the jump of the normal component of the current density across the E-layer, $[j_z] = j_z(L+0) - j_z(L-0)$, and Σ_P is the height-integrated Pedersen conductivity.

The region $z > L$ above the E layer is supposed to consist of cold collisionless plasma, where the parallel (field-aligned) conductivity tends to infinity, $\sigma_\parallel \to \infty$. In this region, the potential φ does not depend on z because of the "frozen-in" condition along the geomagnetic field lines. Applying the thin layer approximation to the magnetically conjugated area of the ionosphere, we obtain the boundary condition in this area, similar to condition (6)

$$j_z(L-0) = -(\Sigma_P + \Sigma_P^*)\hat{\Delta}_r\varphi, \tag{7}$$

where Σ_P^* is the height-integrated Pedersen conductivity of the magnetically conjugated ionosphere. Finally, with account of Eq. (2) we come to the following boundary condition at $z = L$:

$$\sigma_a(L)\frac{\partial\varphi}{\partial z} - j_0(L)\exp\left(-\frac{r^2}{r_0^2}\right) = (\Sigma_P + \Sigma_P^*)\hat{\Delta}_r\varphi, \tag{8}$$

3. Electric field in the atmosphere

In this section we provide a solution for the derived above system of equations, augmented with the boundary conditions. First, we consider the situation when the extrinsic current density is maximal in the surface layer of the atmosphere. The extrinsic current is supposed to be driven by the movement of charged aerosols or light ions, which are carried upward from the ground surface by ascending air flows. In this case the altitude dependence of the extrinsic current can be approximated as follows:

$$j_0(z) = j_m \exp(-z/h), \tag{9}$$

where j_m and h are the amplitude and the vertical scale of the current density, respectively.

The solution of Eqs. (4) and (5) with the boundary conditions at $z = 0$ and $z = L$ has been obtained using Hankel transform with respect to variable r as described in Appendix 1. This solution contains a small parameter $\upsilon = \sigma_0/\sigma_g$. Indeed, the conductivity of the upper layers of the Earth's crust σ_g =10^{-3}-10^{-2} S/m is much greater than the atmospheric conductivity at the ground level σ_0 ~10^{-14} S/m. Now we apply the inverse Hankel transform to solution (A1.5) with coefficients (A1.10) and (A1.11), and neglect the terms, which contain the small factor υ. As a result, we obtain the spatial distribution of the atmospheric electric potential ($0 < z < L$):

$$\varphi(r,z) = \frac{j_m r_0^2}{2\sigma_0}\int_0^\infty f(k,z)\exp\left(-\frac{k^2 r_0^2}{4}\right)\frac{k}{s}\mathrm{J}_0(kr)dk. \tag{10}$$

Here we have introduced the following k-functions:

$$\begin{aligned} f(z,k) &= \frac{a_+\exp(\lambda_- z) - a_-\exp(\lambda_+ z)}{2u} - \exp(-\beta z),\\ a_\pm(k) &= (\lambda_\pm + Hk^2)\exp(\pm\xi L) + (h-H)k^2\exp(-\alpha L),\\ u(k) &= \xi\cosh(\xi L) + [Hk^2 - (2l)^{-1}]\sinh(\xi L),\\ \lambda_\pm(k) &= -\frac{1}{2l} \pm \xi, \quad \xi = \left(\frac{1}{4l^2} + k^2\right)^{1/2}, \quad s = \beta - hk^2. \end{aligned} \tag{11}$$

Additionally, we used the following notations

$$\alpha = \frac{1}{2l} + \frac{1}{h}, \quad \beta = \frac{1}{l} + \frac{1}{h}, \quad H = \frac{\Sigma_P + \Sigma_P^*}{\sigma_a(L)}. \tag{12}$$

Note that the function $s(k)$ in the denominator of Eq. (10) vanishes at the point $k = (\beta/h)^{1/2}$. Nevertheless, the integrand has no singularity since the function $f(k,z)$ in its numerator vanishes at the same point. Using Eq. (10) one can find the electric field components:

$$E_z = \frac{j_m r_0^2}{2\sigma_0}\int_0^\infty \left\{\frac{a_-\lambda_+\exp(\lambda_+ z) - a_+\lambda_-\exp(\lambda_- z)}{2u} - \beta\exp(-\beta z)\right\}\exp\left(-\frac{k^2 r_0^2}{4}\right)\frac{k}{s}\mathrm{J}_0(kr)dk, \tag{13}$$

$$E_r = \frac{j_m r_0^2}{2\sigma_0}\int_0^\infty f(k,z)\exp\left(-\frac{k^2 r_0^2}{4}\right)\frac{k^2}{s}\mathrm{J}_1(kr)dk, \tag{14}$$

where $\mathrm{J}_0(x)$ and $\mathrm{J}_1(x)$ are Bessel functions.

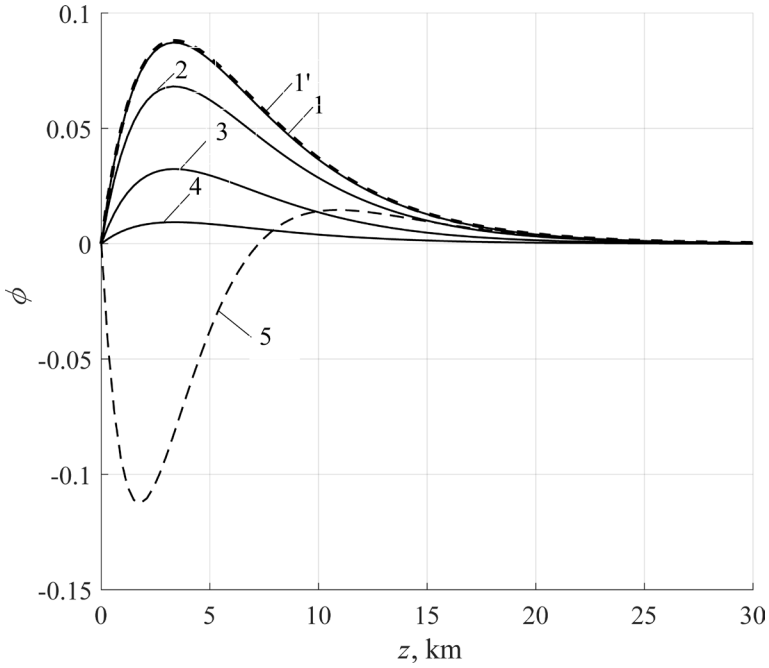

Figure 2. Dimensionless electric potential in the atmosphere as a function of altitude z for fixed distances from z-axis: $r = 0$, 50, 100 and 150 km (denoted by solid lines 1-4, respectively). Here we have used the parameters $\sigma_0 = 10^{-14}$ S/m, $r_0 = 100$ km, $h = 10$ km, $l = 4$ km, $L = 80$ km, and $h_0 = 5$ km. The calculation results obtained with approximate Eqs. (18) and (19) are shown with dashed line 1′.

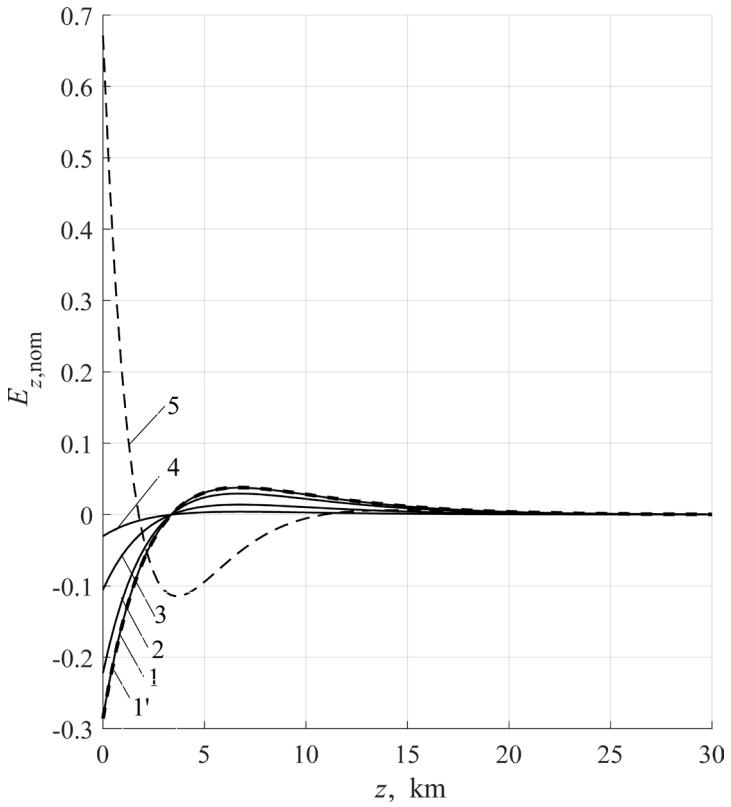

Figure 3. Dimensionless vertical component of the electric field in the atmosphere as a function of altitude z for fixed distances from z-axis: $r_0 = 0, 50, 100$ and 150 km (denoted by solid lines 1-4, respectively). The calculation results obtained with approximate Eqs. (18) and (19) are shown with dashed line 1′.

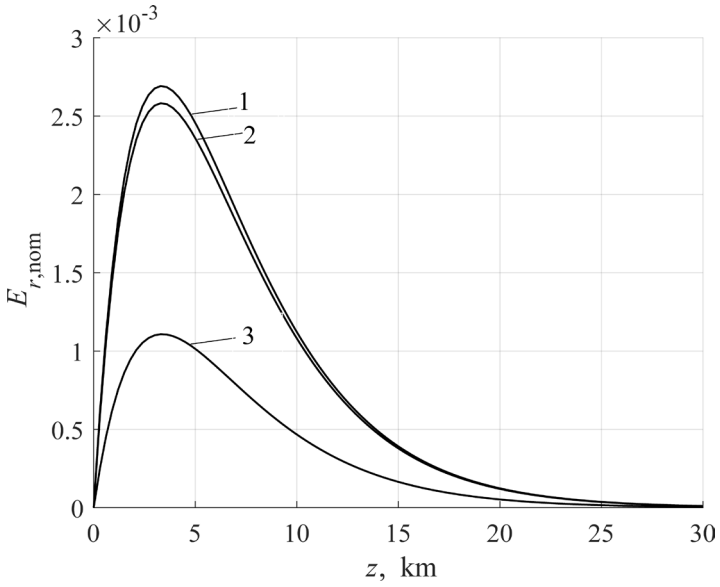

Figure 4. Dimensionless horizontal component of the electric field in the atmosphere as a function of altitude z. The graphs 1-3 correspond to the radii $r = 50$, 100, and 150 km, respectively.

To illustrate the dependence of the electric field on altitude, numerical calculations have been performed for the following parameters. The characteristic transverse scale of the extrinsic current amounts to tens-hundreds of km. The parameter l is of the order of several km. The parameter h can vary from several km to tens of km depending on the model of the extrinsic current. Therefore, we perform calculation for reasonable parameters: $\sigma_0 = 10^{-14}$ S/m, $r_0 = 100$ km, $h = 10$ km, $l = 4$ km, $L = 80$ km, $\Sigma_P = \Sigma_P^* = 0.5$ S (nighttime ionosphere). Figure 2 shows the dependence of the dimensionless potential $\phi = \varphi\sigma_0/j_m l$ on altitude z at several fixed distances from z-axis.

In Figure 3 we plot the altitude dependence of the dimensionless vertical component of the atmospheric electric field $E_{z,\mathrm{nom}} = E_z\sigma_0/j_m$ for the same radii. The peculiarity of these dependencies is that the electric field is concentrated mainly near the ground surface in a layer with a thickness of ~10 km. This size is about the characteristic scale h of the extrinsic current decrease.

The altitude dependence of the dimensionless horizontal component of electric field in the atmosphere $E_{r,\mathrm{nom}} = E_r\sigma_0/j_m$ is shown in Figure 4 for several radii. This figure shows that in the atmosphere the horizontal component of E-field is almost two orders of magnitude smaller than the vertical component throughout all heights.

3.1 Simplified quasi-1D consideration

In what follows we give a simple interpretation of the above solution for the atmosphere. We consider a wide distribution of the extrinsic current when its transverse scale r_0 is comparable or even greater than the distance L between the ground and ionosphere. Then, one can find an approximate solution for the potential for distances $r \ll r_0$. Figures 3 and 4 show that $|E_z| \gg |E_r|$ within this radius interval. Therefore, in the first approximation, the horizontal current is negligible as compared with the vertical one, and all the functions depend on z only. In this case, the stationary continuity equation for the total current is reduced to the following 1D form

$$\frac{d}{dz}\left(-\sigma_a(z)\frac{d\varphi}{dz} + j_0(z)\right) = 0. \tag{15}$$

Upon integration of this equation along z, we obtain

$$-\sigma_a(z)\frac{d\varphi}{dz} + j_0(z) = j_{\mathrm{tot}}, \tag{16}$$

where j_{tot} is the density of the total electric current, which includes both the extrinsic and conduction currents.

As follows from solution (10), the ground conductivity has little effect on the electric potential, so we assume that the ground is an ideal conductor. Inserting the function $\sigma_a = \sigma_0 \exp(z/l)$ into Eq. (16) and performing the integration of this equation under the boundary requirement $\varphi(0) = 0$, we arrive at

$$\varphi(z) = \frac{1}{\sigma_0}\int_0^z j_0(z')\exp\left(-\frac{z'}{l}\right)dz' - \frac{j_{\text{tot}}l}{\sigma_0}\left\{1 - \exp\left(-\frac{z}{l}\right)\right\}. \tag{17}$$

The approximate solutions for the potential $\varphi(z)$ and electric field $E_z(z) = -\,d\varphi/dz$ are as follows:

$$\varphi(z) = \frac{j_m}{\sigma_0\beta}\{1 - \exp(-\beta z)\} - \frac{j_{\text{tot}}l}{\sigma_0}\left\{1 - \exp\left(-\frac{z}{l}\right)\right\}, \tag{18}$$

$$E_z(z) = \frac{1}{\sigma_0}\left\{j_{\text{tot}} - j_m \exp\left(-\frac{z}{h}\right)\right\}\exp\left(-\frac{z}{l}\right). \tag{19}$$

The constant j_{tot} may be found from Eq. (18) under the boundary condition $\varphi(L) = 0$

$$j_{\text{tot}} = \frac{j_m}{(1 + l/h)}\left\{\frac{1 - \exp(-\beta L)}{1 - exp(-L/l)}\right\}. \tag{20}$$

The calculation results obtained with approximate Eqs. (18) and (19) are shown in Figures 2 and 3 with dashed lines. These results are very close to the results of calculations using more precise Eqs. (10) and (13) for $r = 0$ shown with solid lines. Approximate Eqs. (18) and (19) can reasonably well approximate the potential and electric field for other values of r if these formulas were multiplied by the factor $\exp(-r^2/r_0^2)$.

Figure 5a shows the altitude dependence of the dimensionless extrinsic current j_0/j_m, conductivity current $\sigma_a(z)\,E_z/j_m$, and total current j_{tot}/j_m. The extrinsic current decreases with altitude in accordance with Eq. (9), whereas the conductivity current increases in such a way to make the total current constant. Thus, the conductivity current density tends asymptotically to the value j_{tot} given by Eq. (20).

The approximate equations obtained above provide a possibility to estimate the relationship between the external current and electric field at the interface ground-atmosphere and atmosphere-ionosphere. For realistic parameters $\exp(-L/l) \ll 1$ and $\exp(-L/h) \ll 1$, and these relationships simplify to the following

$$E_z(0) \approx -\frac{j_m l}{\sigma_0(l + h)} \quad E_z(L) \approx \frac{j_m h}{\sigma_a(L)(l + h)}. \tag{21}$$

From these estimates it follows that the atmospheric electric field attenuates with altitude exponentially at high altitudes because $E_z(z) \approx j_{\text{tot}}\sigma_a^{-1}(z) \propto \exp(-z/l)$ (Figure 5a).

3.2 Extrinsic current originating well above the ground

The extrinsic current caused by charged atmospheric aerosols may reach its maximum at some altitude above the ground. For this case, instead of Eq. (9), the dependence of the extrinsic current on altitude can be modeled as

$$j_0(z) = (j_m z/h_0)\exp(1 - z/h_0). \tag{22}$$

This function reaches a peak value j_m at $z = h_0$. To derive an expression for the electric field resulted from this kind of extrinsic current, we consider again the case $r \ll r_0$. For the current described by Eq. (22), the solution of Eq. (17) is as follows

$$\varphi(z) = \frac{j_m \mathrm{e}}{\sigma_0 h_0 \beta_0^2}\{1 - (1 + \beta_0 z)\exp(-\beta_0 z)\} - \frac{j_{\mathrm{tot}} l}{\sigma_0}\left\{1 - \exp\left(-\frac{z}{l}\right)\right\}, \tag{23}$$

$$E_z(z) = \frac{1}{\sigma_0}\left\{j_{\mathrm{tot}} - j_m \frac{z\mathrm{e}}{h_0}\exp\left(-\frac{z}{h_0}\right)\right\}\exp\left(-\frac{z}{l}\right). \tag{24}$$

where $\beta_0 = l^{-1} + h_0^{-1}$. As before, taking into account the requirement $\varphi(L) = 0$, we obtain the total current:

$$j_{\mathrm{tot}} = \frac{j_m \mathrm{e}}{(l + h_0)\beta_0}\left\{\frac{1 - (1 + \beta_0 L)\exp(-\beta_0 L)}{1 - \exp(-L/l)}\right\}, \tag{25}$$

a)

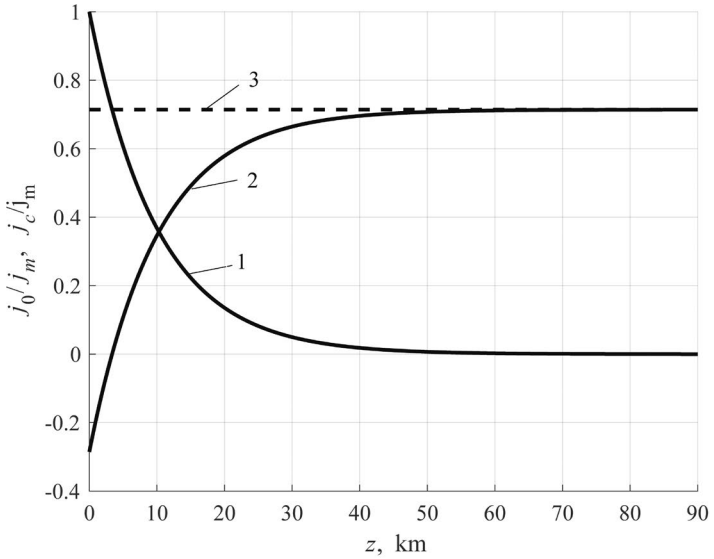

b)

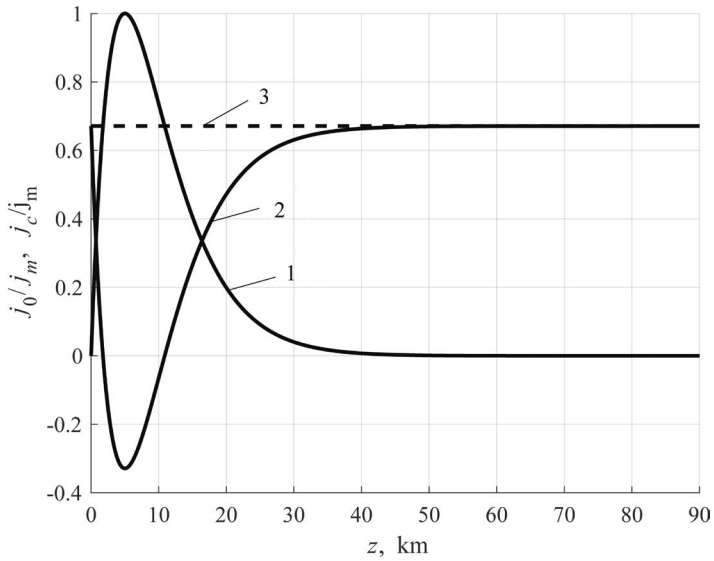

Figure 5. Altitude dependences of dimensionless extrinsic current density, conduction current, and total current are shown by lines 1-3, correspondingly. The external current was chosen to be maximal at the ground surface (top panel) or at some altitude above the ground (bottom panel).

The dimensionless potential $\phi = \varphi\sigma_0/(j_m l)$ and electric field $E_{z,\mathrm{nom}} = E_z\sigma_0/j_m$ calculated from Eqs. (23) and (24) are shown in Figures 2 and 3 with lines 5. In the lower atmosphere, the graph for the current model (22) has an opposite polarity as compared with graphs for the current model (9). This distinction is related to the following feature. For the extrinsic current described by Eq. (9), the disturbed electric field on the ground is $E_z(0) = (j_{\mathrm{tot}} - j_m)/\sigma_0$. From Eq. (20) it follows that $j_m > j_{\mathrm{tot}}$, and pertinent graphs in Figure 3 are negative $E_z(0) < 0$. At the same time the extrinsic current described by Eq. (22) vanishes on the ground surface. In this case $E_z(0) = j_{\mathrm{tot}}/\sigma_0 > 0$, hence the corresponding graph in Figure 3 is positive.

A common feature of all graphs is that the electric field is mainly concentrated near the ground surface, and at altitudes above 10 km decreases sharply. From Eqs. (23) and (24) simple relationships follow for the electric field near the ground $E_z(0) \approx j_{\mathrm{tot}}/\sigma_0$ and beneath the ionosphere $E_z(L) \approx j_{\mathrm{tot}}/\sigma_a(L)$. These simplified relationships provide estimates of the same order as Eq. (21).

Figure 5b shows the altitude dependence of the dimensionless external current, conductivity, and total current, as follows from Eqns. (23-25). This figure demonstrates the same tendency as Figure 5a does, that at high altitudes the conductivity current density tends asymptotically to the value j_{tot}, given by Eq. (25). Thus, for any model of the external current the electric field rapidly decays with altitude in such a way that $E_z(0) \gg E_z(L)$. In the next section we show that spreading of currents across the E-layer results in an additional decay of the electric field amplitude in the ionosphere.

4. Electric field in the ionosphere

In order to find the electric field in the E-layer, one should take into account that the horizontal electric field must be continuous at the boundary between the atmosphere and ionosphere ($z = L$). In the thin layer approximation, the ionospheric radial field E_r can be found from Eq. (14). The vertical electric field experiences a jump $[E_z] = E_z(L+) - E_z(L-)$ at this boundary, and the vertical field near the lower boundary of the ionosphere $E_z(L-) = E_z(r, L)$ is given by Eq. (13).

The continuity requirement for the normal component of the current density at the atmosphere-ionosphere boundary is $\sigma_a(L)E_z(L-) \approx \sigma_\parallel E_z(L+)$, taking into account that there the extrinsic current is much smaller than the conduction current. From this boundary condition it follows that $E_z(L+) \ll E_z(L-)$ since the parallel plasma conductivity $\sigma_\parallel$ is several orders of magnitude greater than $\sigma_a(L)$. Therefore, the vertical electric field in the ionosphere can be neglected, i.e. $E_z(L+) \to 0$.

The atmospheric resistance and the extrinsic current caused by the charged aerosols or radon emission are mainly concentrated in the bottom atmosphere. This implies that the conditions $L \gg 2l$ and $L \gg h$ are fulfilled, which enables one to simplify the equations for $E_r(r,L)$ and $E_z(r,L)$. If the characteristic transverse size of the extrinsic current is comparable to or larger than L and is much greater than other scales, $r_0 \gg h, l$, then the equations for the electric field are further simplified. For this case the corresponding approximate equations are given in Appendix 2. Rearranging Eqs. (A2.6) and (A2.7), we find that

$$E_z(r, L-) = E_z(r, L) \approx \frac{j_m}{\sigma_a(L)(1 + l/h)(1 + l/H)(1 + 4lL/r_0^2)} \exp\left(-\frac{r^2}{r_0^2 + 4lL}\right), \tag{26}$$

$$E_r(r, L) \approx \frac{j_m r_0^2}{2(1 + l/h)(1 + l/H)(\Sigma_P + \Sigma_P^*)r} \left\{1 - \exp\left(-\frac{r^2}{r_0^2 + 4lL}\right)\right\}. \tag{27}$$

The equation (26) determines the vertical field in the atmosphere near the interface with the ionosphere ($z = L$–), while Eq. (27) determines the horizontal field in the E-layer.

Figure 6 shows the dimensionless vertical and horizontal components of the electric field $E_{z,\mathrm{nom}} = E_z(L-)\,\sigma_a(L)/j_m$ and $E_{r,\mathrm{nom}} = E_r(\Sigma_P + \Sigma_P^*)/(j_m r_0)$ calculated for the nighttime ionosphere from the exact Eqs. (13) and (14) (solid lines) and approximate Eqs. (26) and (27) (dashed lines). The plots for daytime conditions differ from those for nighttime by not more than a few % (not shown). However, in dimensional units, the horizontal field E_r during nighttime is higher than that during daytime due to the factor $1/(\Sigma_P + \Sigma_P^*)$. The nighttime Pedersen conductance

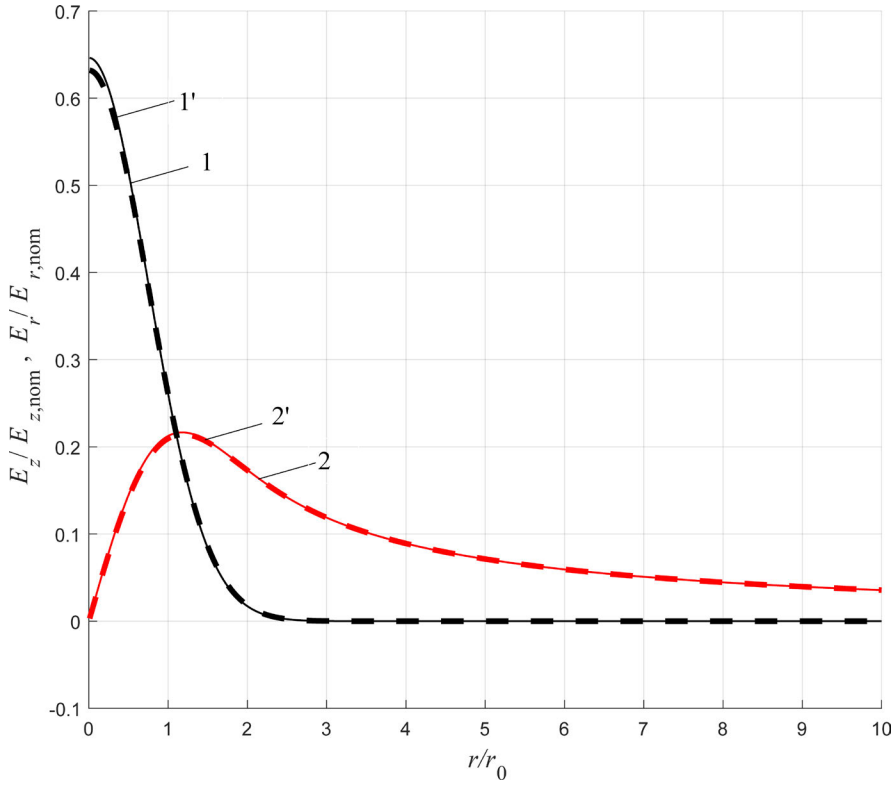

Figure 6. Dimensionless vertical and horizontal components of the electric field as functions of the horizontal distance to the z-axis. The atmospheric vertical field at the boundary of the atmosphere and ionosphere is shown with lines 1 and 1′. The horizontal field in the E-layer of the ionosphere is shown with red lines 2 and 2′. Here we have used the same parameters as in Figures 1-3, and $\Sigma_P = \Sigma_P^* = 0.5$ S. The results obtained with the exact Eqs. (13) and (14) are shown with solid lines 1 and 2, and results stemming from approximate Eqs. (26) and (27) are shown with dashed lines 1′ and 2′.

is about order of magnitude smaller than that of the daytime ionosphere, therefore the nighttime horizontal field is an order of magnitude larger than that during daytime.

Figure 7 shows the spatial structure of the excited currents. The radial current spreading along the E-layer, $j_r(L) = \sigma_P E_r$, is found using the formula (7). The vertical current flowing from the E-layer into the magnetosphere is found from boundary conditions (6) and (7) as $j_z(L+0) = \Sigma_P^* r^{-1} \partial\,(rE_r)/\partial\, r$. The vertical current is concentrated in the region $r < (r_0^2 + 4lL)^{1/2}$. The horizontal spreading of current along the E-layer prevails at large distances r. The decrease of the j_r and E_r amplitudes $\propto r^{-1}$ is determined predominantly by the geometrical factor.

Analysis of Eq. (27) shows that the horizontal field reaches its peak value $E_{r,\max}$ at the radius $r_{\max} = \gamma(r_0^2 + 4lL)^{1/2}$ (where $\gamma \approx 1.209$)

$$E_{r,\max} = E_r(r_{\max}, L) = \frac{j_m r_0^2 \{1 - \exp(-\gamma^2)\}}{2r_{\max}(1 + l/h)(1 + l/H)(\Sigma_P + \Sigma_P^*)}. \tag{28}$$

For comparison, we find the ratio between the maximum electric field in the ionosphere $E_{r,\max}$ and the maximum of the atmospheric vertical field $E_{z,\max} = E_z(0)$ at $r = 0$ on the ground. Using Eq. (21) we obtain

$$\frac{E_{\mathrm{ion}}}{E_{\mathrm{atm}}} = \frac{E_{r,\max}}{E_{z,\max}} = \frac{\sigma_0 h r_0^2 \{1 - \exp(-\gamma^2)\}}{2\gamma l\{\Sigma_P + \Sigma_P^* + \sigma_a(L) l\}(r_0^2 + 4lL)^{1/2}}. \tag{29}$$

Here we have introduced the notations E_{atm} and E_{ion} for the corresponding maximum values of the fields. The ratio $E_{\mathrm{ion}}/E_{\mathrm{atm}}$ depends not only on the contrast between the atmospheric conductivities at z = 0 and z = L, but also

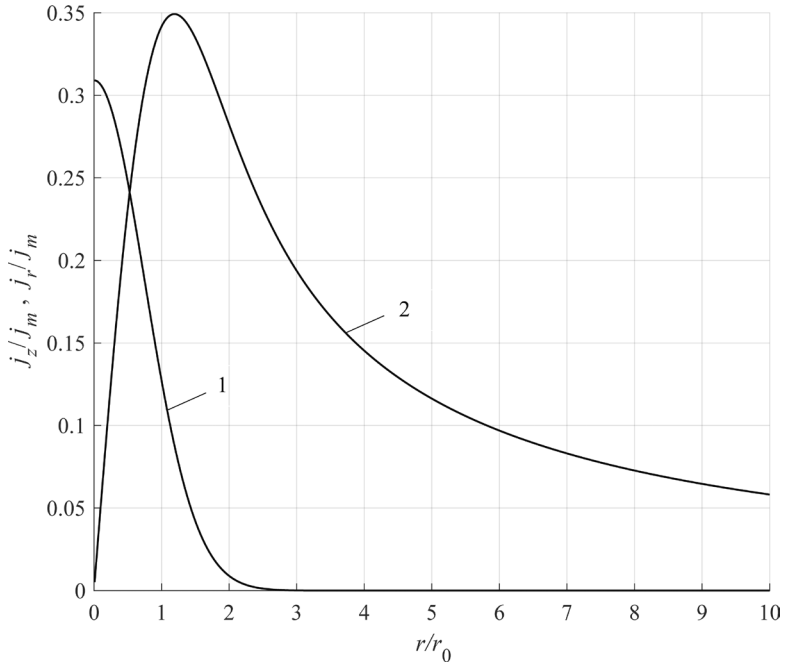

Figure 7. Dimensionless current density in the ionosphere depending on the dimensionless distance to the atmospheric current axis. Line 1 denotes the density of the vertical current flowing from the E-layer into the magnetosphere. Line 2 shows the distribution of the horizontal current spreading along the E-layer.

on the ionospheric height-integrated Pedersen conductance. At the same time, it does not depend on the extrinsic current amplitude. Substituting the above atmospheric and nighttime ionospheric parameters into Eq. (29), we get $E_{\text{ion}}/E_{\text{atm}} \approx 7 \cdot 10^{-10}$. For daytime conditions, this ratio is even smaller by an order of magnitude, because the daytime Pedersen conductance is larger by about order of magnitude.

Eq. (29) admits an evident interpretation which is based on the simple consideration of the problem illustrated in Figure 8. The total current I flowing from the atmosphere into the ionosphere through its lower boundary has the cross-section $\sim\pi r_0^2$. The current magnitude can be estimated as follows $I \sim \pi r_0^2 j_{\text{tot}} \approx \pi\sigma_0 E_{z,\max} r_0^2 h/l$. Let l_0 be a thickness of the E-layer of both conjugated ionospheres. The current I flowing into the ionosphere from the atmosphere partially spreads along the conductive E-layer through the lateral surface of the cylinder with radius r_0 and height l_0, and is loss-free transferred in part by field-aligned currents into the conjugate ionosphere. The appropriate balance of these currents is given by

$$I \sim 2\pi r_0 l_0 \sigma_P E_{r,\max} + 2\pi r_0 l_0 \sigma_P^* E_{r,\max} \sim 2\pi r_0 (\Sigma_P + \Sigma_P^*) E_{r,\max}. \tag{30}$$

Equating the above expression for the current I to Eq. (30) we obtain the estimate

$$\frac{E_{\text{ion}}}{E_{\text{atm}}} \sim \frac{\sigma_0 h r_0}{2l(\Sigma_P + \Sigma_P^*)}. \tag{31}$$

This expression coincides by order of magnitude with Eq. (29) for a sufficiently wide distribution of the extrinsic current, i.e., under the conditions $r_0^2 \gg 4lL$ and $\Sigma_P + \Sigma_P^* \gg \sigma_a(L)l$. The above analysis has shown that spreading of the current across the E-layer results in an additional decrease of the E-field magnitude.

Formally, the estimates obtained above are valid only for the polar ionosphere. For an inclined geomagnetic field the problem will not be axially symmetric even for a vertical atmospheric current. The spreading of currents along the E-layer and the electric field distribution will no longer be axially symmetric. The excited field aligned current will be guided by an inclined $\mathbf{B}_0$, and electric field, carried by shear Alfvén waves along the geomagnetic

field lines, will change. Nevertheless, the account for the geomagnetic field inclination will not modify the results considerably, the current and field magnitudes will be nearly the same, and the order of magnitude of E_{ion}/E_{atm} factor will retain its former value.

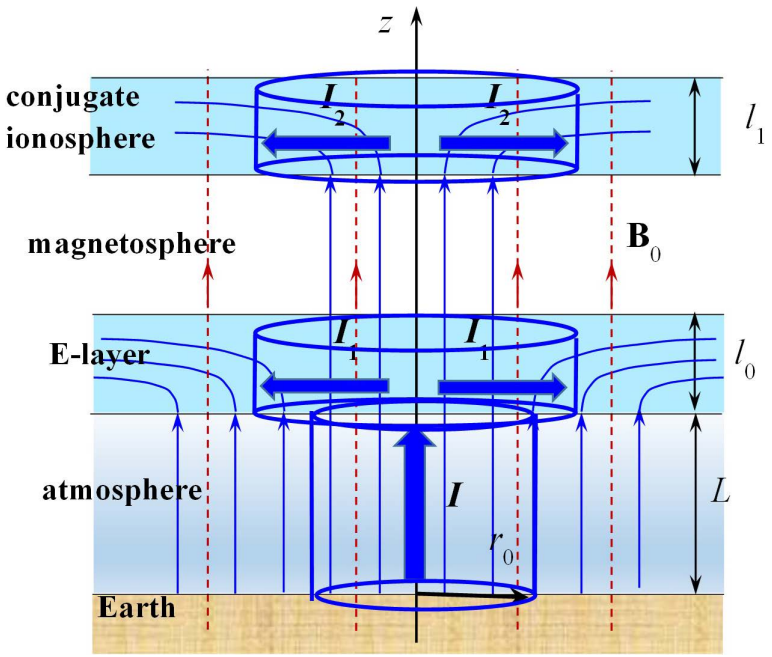

Figure 8. Simplified illustration of the physical process under consideration.

5. Discussion

Here we have focused on the hypothesis that the extrinsic currents of seismogenic origin can transfer electric field perturbations from the lower atmosphere to the ionosphere. This hypothesis was used to interpret ionospheric anomalies as precursors of impending earthquakes. The main conclusion about the rate of the E-field penetration into the ionosphere follows from the simple fact that the density of the total vertical current in the atmosphere j_{tot}, which includes the conduction and extrinsic currents, practically does not depend on the height. At high altitudes, where the extrinsic current becomes negligible, the conduction current dominates, i.e. $\sigma_a E_z \approx j_{tot}$. Whence a sharp increase in the atmospheric conductivity with altitude leads to an almost exponential decrease in the vertical component of the electric field perturbation in accordance with estimates (19) and (24).

Upward transfer of the charged aerosols by atmospheric convection and their gravitational sedimentation results in the formation of EMF. Let us dwell, for example, on a model in which the extrinsic current has a maximum on the earth's surface. Using Eq. (16) one can obtain the following relation between the vertical electric fields at the lower edge of the ionosphere and on the ground $E_z(L) = \{\sigma_0 E_z(0)/\sigma_a(L)\}(1+\xi)$, where $\xi = j_m/[\sigma_0 E_z(0)]$ (Sorokin and Hayakawa 2013). If we assume that $\xi \gg 1$, then this expression is simplified to the form: $E_z(L) \approx j_m/\sigma_a(L)$. If we take an external current j_m=10^{-7} A/m^2, i.e. about 5 orders of magnitude greater than the fair weather current, then from this estimate we obtain the value $E_z(L)$~10 mV/m. This value is about the pre-seismic electric field disturbances sometimes observed on satellites (Chmyrev et al. 1989; Gousheva et al. 2009; Liu and Chao 2017). This consideration seemingly shows that the aerosol upward current could be a very effective generator of the ionospheric electric field disturbance, as was suggested in (Sorokin et al. 2007; Namgaladze and Karpov 2015; Namgaladze et al. 2018).

However, in reality the inequality $\xi \gg 1$ on which the above estimate of $E_z(L)$ is based does not hold. The reason for this is that the parameters j_m and $E_z(0)$ cannot be treated as independent variables. They are coupled owing to the boundary conditions for the potential and current density on the ground and in the ionosphere. For example, from equation (21), which takes these relationships into account, it follows that $\xi = -(1 + h/l) = -3.5$. Substituting this expression for ξ into the above formula, we obtain a correct estimate: $E_z(L)/E_z(0) \approx -\sigma_0 h/\sigma_a(L) l$. In the model where

the extrinsic current reaches its maximum value at a certain height h_0, we find similarly $\xi = (l + h_0)^2/(\mathrm{e}lh_0) = 1.5$. Hence the electric field in the atmosphere decreases with height as $E_z(L)/E_z(0) \propto \sigma_0/\sigma_a(L)$. The atmospheric conductivity becomes anisotropic at altitude $L \sim 80$ km, where $\sigma_a(L) \sim 1.6 \cdot 10^{-5}$ S/m during daytime, and $\sigma_a(L) \sim 7 \cdot 10^{-9}$ S/m during nighttime. Therefore, the atmospheric E-field attenuation rate may vary around 10^{-9}-10^{-6}.

In the previous section, a more precise analysis has been carried out, taking into account the effect of current spreading in the ionosphere. This analysis has shown that the ratio of the electric field amplitudes in the ionosphere and on the earth's surface is determined by Eq. (29), from which it follows that $E_{\mathrm{ion}}/E_{\mathrm{atm}} \propto \sigma_0 h/\{\Sigma_P + \Sigma_P^* + \sigma_a(L)l\}$. In this relation, $\sigma_0 h$ is the height-integrated conductivity of the lower atmospheric layer, where the extrinsic current is located, and $\Sigma_P + \Sigma_P^* + \sigma_a(L)l$ is the sum of the height-integrated conductivities of the ionospheres and the upper layer of the atmosphere. For typical parameters we arrive to the estimate $E_{\mathrm{ion}}/E_{\mathrm{atm}} \approx 7 \cdot 10^{-10}$ for the nighttime ionosphere, whereas for daytime conditions this estimate is an order of magnitude lower.

We need to clarify another issue: what magnitude of electrical perturbations generated by the extrinsic current in the lower atmosphere would be necessary to produce the E-field response in the ionosphere about the perturbations measured by LEO satellites? For example, the disturbance $E_{\mathrm{ion}} \sim 1$ mV/m was recorded onboard the FORMOSAT-5 satellite before M = 6.8 earthquake [Liu and Chao 2017]. As follows from our model, to produce E-field disturbance in the nighttime ionosphere with such amplitude an atmospheric electric field with amplitude $E_{\mathrm{atm}} \sim 1.4 \cdot 10^6$ V/m is necessary. This value is about 4 orders of magnitude greater than the usual atmospheric electric field near the earth's surface and is close to the electric discharge threshold $3.2 \cdot 10^6$ V/m at normal atmospheric pressure. The extrinsic current density on the ground, which corresponds to this field, is $j_m \approx \sigma_0(1 + h/k)E_{\mathrm{atm}} \approx 5 \cdot 10^{-8}$ A/m^2. Similar estimates can be obtained for another model in which the extrinsic current reaches its peak at some altitude above the ground. Before some earthquakes, an anomalous increase in the atmospheric field up to $E_{\mathrm{atm}} = 350$-700 V/m was observed, which could be caused by an extrinsic current of seismogenic origin [Hao et al. 2000]. According to the above estimates, this effect is to be accompanied by the DC electric field disturbances in the ionosphere $E_{\mathrm{ion}} = 0.25$-0.5 μV/m. This value is below the threshold of natural ionospheric fluctuations. A similar conclusion was made on the basis of the numerical modeling of atmospheric and ionospheric currents caused by a given current source on the Earth's surface [Kuo et al. 2014]. According to these numerical calculations, in order to obtain an electric field in the ionosphere of the order of several mV/m, it is necessary to have at the Earth's surface a source with current density $\sim 10^{-7}$ A/m^2. The associated electric field must be ~500 kV/m, that is 3-4 order of magnitude greater than the fair-weather electric field. Thus, both analytical estimates and numerical modeling prove that the hypothesis of the aerosol current as a mechanism of the ionospheric precursors looks far from reality.

However, we do not insist that the channel of LAIC via the atmospheric electric field must be disregarded completely. As compared with DC field, the non-stationary electric field penetrate the conductive upper atmosphere more easily although the non-stationary electric field cannot cause significant perturbations of electron density in F2-region of the ionosphere (Park and Dejnakarintra 1973; Mazur et al. 2023). Therefore, pre-earthquake anomalies in the form of sporadic sequence of near-ground E-field pulses could be more efficient LAIC factor than DC field.

6. Conclusion

In this study, a general model of the electric field produced by a vertical extrinsic current in the lower atmosphere has been elaborated. This current may be associated with the upward convection of charged aerosols or the emanation of radioactive radon gas from the soil. Theoretical consideration has shown that the perturbations of the atmospheric electric field caused by such current are concentrated mainly in the lower atmosphere. In this region the vertical component of electrical perturbation is about two orders of magnitude greater than the horizontal component. At altitudes above 10-15 km, the electric field perturbations decrease with altitude almost exponentially with the same characteristic scale l as conductivity variations (several km). The vertical atmospheric current flowing into the ionosphere through its lower boundary partially spreads along the conductive E-layer and is partially transferred along the geomagnetic field lines into the magnetically conjugate ionosphere. An additional field decrease in the E-layer of the ionosphere occurs due to the horizontal spreading of currents. The electric field in the ionosphere has been estimated in the "thin layer" approximation. Approximate analytical expressions have been derived that determine the relationship between the amplitudes of electrical disturbances in the atmosphere E_{atm} and ionosphere E_{ion}. The value $E_{\mathrm{ion}}/E_{\mathrm{atm}}$ is proportional to the ratio of the integral conductivity of the lower layer of the atmosphere to the sum of the height-integrated conductivity of the upper atmosphere and ionosphere.

Within the framework of the model, the ratio E_{ion}/E_{atm} is about 10^{-9} and it does not depend on the extrinsic current amplitude. For daytime conditions, this value is even less by 1-2 orders of magnitude. Therefore, the hypothesis that ionospheric disturbances ~1-10 mV/m could be caused by seismogenic upward aerosol flow requires unrealistically large values of E_{atm} and seems unlikely. So, it is necessary to examine other physical mechanisms to explain the LAIC phenomena.

Appendix 1.

The use of the Hankel transform of Eqs. (4), (5) and boundary condition (8) in respect to variable r yields

$$\psi'' - k^2\psi = 0, \quad (z < 0); \tag{A1.1}$$

$$\psi'' + \frac{\psi'}{l} - k^2\psi = \frac{j_0'(z)r_0^2}{2\sigma_0}\exp\left(-\frac{k^2r_0^2}{4} - \frac{z}{l}\right), \quad (0 < z < L); \tag{A1.2}$$

$$\psi' + D\psi = \frac{j_0(L)r_0^2}{2\sigma_a(L)}\exp\left(-\frac{k^2r_0^2}{4}\right), \quad (z = L); \tag{A1.3}$$

where $D = k^2(\Sigma_P + \Sigma_P^*)/\sigma_a(L)$, k is the transform parameter, and the primes denote derivatives with respect to z. Here ψ stands for the Hankel transform of the potential

$$\psi(z,k) = \int_0^\infty \varphi(z,r)\mathrm{J}_0(kr)rdr, \tag{A1.4}$$

where $\mathrm{J}_0(x)$ is the Bessel function. Solution of Eq. (A1.1) which attenuates at $z \to -\infty$ is given by $\psi = C_0\exp(kz)$, where C_0 is undetermined coefficient.

Let us substitute Eq. (9) for the function $j_0(x)$ into Eq. (A1.2). Then the general solution of this equation is as follows

$$\psi = C_1\exp(\lambda_+ z) + C_2\exp(\lambda_- z) + A\exp(-\beta z), \tag{A1.5}$$

where C_1 and C_2 are undetermined coefficients. Here we have used the following abbreviations

$$\begin{aligned} &\beta = \frac{1}{l} + \frac{1}{h}, \quad \lambda_\pm = -\frac{1}{2l} \pm \left(\frac{1}{4l^2} + k^2\right)^{1/2}, \\ &A = -\frac{j_m r_0^2}{2\sigma_0 s}\exp\left(-\frac{k^2r_0^2}{4}\right), \quad s = \frac{1}{h} + \frac{1}{l} - hk^2. \end{aligned} \tag{A1.6}$$

The requirements of the continuity for the potential ψ and normal component j_z of the current density at $z = 0$ yield:

$$C_0 = C_1 + C_2 + A, \tag{A1.7}$$

$$\frac{k\sigma_g C_0}{\sigma_0} = C_1\lambda_+ + C_2\lambda_- - \beta A - \frac{j_m r_0^2}{2\sigma_0}\exp\left(-\frac{k^2r_0^2}{4}\right). \tag{A1.8}$$

Substituting Eq. (A1.5) for ψ into the boundary condition (A1.3), we get the following relationship

$$C_1(\lambda_+ + D)\exp(\lambda_+ L) + C_2(\lambda_- + D)\exp(\lambda_- L) = A(hk^2 - D)\exp(-\beta L). \tag{A1.9}$$

Solving the algebraic set of equations (A1.7)-(A1.9) one can find all undetermined coefficients. In particular, the coefficients C_1 and C_2 are

$$C_1 = N_-/w, \quad C_2 = -N_+/w. \tag{A1.10}$$

Here we used the notations

$$\begin{aligned} &N_\pm = A\{k(\lambda_\pm + D)(1 + vkh)\exp(\pm\xi/L) + (hk^2 - D)(k - v\lambda_\pm)\exp(-\alpha L)\}, \\ &w = (\lambda_+ + D)(k - v\lambda_-)\exp(\xi L) - (\lambda_- + D)(k - v\lambda_+)\exp(-\xi L), \\ &v = \frac{\sigma_0}{\sigma_g}, \quad \alpha = \frac{1}{2l} + \frac{1}{h}, \quad \xi = \left(\frac{1}{4l^2} + k^2\right)^{1/2}. \end{aligned} \tag{A1.11}$$

Substituting the above equations for the coefficients C_1 and C_2 into Eq. (A1.5), we obtain the potential ψ of the electric field in the atmosphere ($0 < z < L$) and in the E-layer ($z = L$).

Appendix 2.

The electric field at the interface between the ionosphere and atmosphere ($z = L$) can be found from Eqs. (13) and (14) as follows

$$E_z(r, l) \approx M\int_0^\infty \left\{\frac{p_z k^2}{2lu} - \beta\exp(-\alpha L)\right\}\exp\left(-\frac{k^2 r_0^2}{4}\right)\frac{k}{s}\mathrm{J}_0(kr)dk, \tag{A2.1}$$

$$E_r(r, L) = M\int_0^\infty \left\{\frac{p_r}{u} - \exp(-\alpha L)\right\}\exp\left(-\frac{k^2 r_0^2}{4}\right)\frac{k^2}{s}\mathrm{J}_1(kr)dk. \tag{A2.2}$$

Here we have used the following abbreviations

$$\begin{aligned} &M = \frac{j_m r_0^2}{2\sigma_0}\exp\left(-\frac{l}{2l}\right), \\ &p_z = 2\xi lh + (H - h)\exp(-\alpha L)\{\sinh(\xi L) - 2\xi L\cosh(\xi L)\}, \\ &p_r = \xi + (H - h)\,k^2\exp(-\alpha L)\sin\mathrm{h}\,(\xi L). \end{aligned} \tag{A2.3}$$

Taking into account that $\xi L \geq L/(2l) \gg 1$, we can simplify the integrands by setting $\sinh(\xi L) \approx \cosh(\xi L) \approx \exp(\xi L)/2$. Eqs. (2.1)-(2.3) can be simplified once again for a sufficiently wide horizontal scale of the extrinsic current, i.e. $r_0 \gg h$ and $r_0 \gg 2l$. The presence of the exponential factor $\exp(-k^2 r_0^2/4)$ in the integrand in Eqs. (A2.1) and (A2.2) means

that the integral sums are mostly accumulated in the range $0 \le k < 2/r_0$. In this area, integrands in Eqs. (2.1)-(2.3) can be expanded in power series of the small parameter kl. In the first approximation one can use the following $\xi \approx (2l)^{-1} + lk^2$, $\lambda_+ \approx lk^2$, $\lambda_- \approx -1/l$, and $s(k) \approx \beta$. As a result, we obtain

$$E_z(r,L) \approx \frac{j_m r_0^2}{2\sigma_a(L)} \int_0^\infty \left\{ \frac{\exp(-lLk^2) - (1-h/H)k^2 l^2 \exp(-L/h)}{(1+l/h)(1+l/H)} - \exp\left(-\frac{L}{h}\right) \right\} \exp\left(-\frac{k^2 r_0^2}{4}\right) \mathrm{J}_0(kr) k dk. \quad \text{(A2.4)}$$

$$E_r(r,L) \approx \frac{j_m r_0^2}{2\sigma_a(L)\beta l(H+l)} \int_0^\infty \left\{ \exp(-lLk^2) - l(h+l)k^2 \exp\left(-\frac{L}{h}\right) \right\} \exp\left(-\frac{k^2 r_0^2}{4}\right) \mathrm{J}_1(kr) dk. \quad \text{(A2.5)}$$

Eq. (A2.4) can be represented as a sum of three integrals while Eq. (A2.5) is as a sum of two integrals. These integrals are reduced to tabular integrals (Grandshteyn and Ryzhik 2007, p. 706) that results in

$$E_z(r,L) \approx \frac{j_m}{\sigma_a(L)} \left\{ \frac{\exp\left(-\frac{r^2}{r_0^2+4lL}\right)}{\left(1+\frac{l}{h}\right)\left(1+\frac{l}{H}\right)\left(1+\frac{4lL}{r_0^2}\right)} - \left[q + (1-q)\frac{r^2}{r_0^2}\right] \exp\left(-\frac{L}{h} - \frac{r^2}{r_0^2}\right) \right\}, \quad \text{(A2.6)}$$

$$E_r(r,L) \approx \frac{j_m r_0^2}{2(1+l/h)(1+l/H)(\Sigma_P + \Sigma_P^*)r} \left\{ 1 - \exp\left(-\frac{r^2}{r_0^2+4lL}\right) - \frac{4l(h+l)r^2}{r_0^4} \exp\left(-\frac{h}{L} - \frac{r^2}{r_0^2}\right) \right\}, \quad \text{(A2.7)}$$

where

$$q = 1 + \frac{4l^2}{r_0^2} \frac{(1-h/H)}{(1+l/h)(1-l/H)}. \quad \text{(A2.8)}$$

Funding. This study is supported by the grant No 22-17-00125 from the Russian Science Foundation.

Author statement. The authors have no relevant financial or non-financial interests to disclose. VS performed theoretical calculations, graph plotting and wrote the original draft. VP performed conceptualization, supervision, project administration, and editing.

References

Astafyeva, E. (2019). Ionospheric detection of natural hazards, Rev. Geophys., 57, 1265-1288. https://doi.org/10.1029/2019RG000668

Chmyrev, V.M., N.V. Isaev, S.V. Bilichenko, and G.A. Stanev (1989). Observation by space – borne detectors of electric fields and hydromagnetic waves in the ionosphere over an earthquake center, Phys. Earth Planet. Inter., 57, 110-114, http://dx.doi.org/10.1016/0031-9201(89)90220-3

Chowdhury, S., A. Deb, C. Barman, et al. (2022). Simultaneous monitoring of soil ^{222}Rn in the Eastern Himalayas and the geothermal region of eastern India: an earthquake precursor, Nat. Hazards, 112, 1477-1502, https://doi.org/10.1007/s11069-022-05235-9

Cigolini, C., M. Laiolo and D. Coppola (2015). The LVD signals during the early-mid stages of the L'Aquila seismic sequence and the radon signature of some aftershocks of moderate magnitude. J. Environ. Radioactivity, 139 56-65, doi:10.1016/j.jenvrad.2014.09.017

Dautermann, T., E. Calais, J. Haase and J. Garrison (2007). Investigation of ionospheric electron content variations before earthquakes in southern California 2003-2004, J. Geophys. Res., 112, B02106, https://doi.org/10.1029/2006JB004447.

Denisenko, V.V., M. Ampferer, E.V. Pomozov, A.V. Kitaev, W. Hausleitner, G. Stangl and H.K. Biernat (2013). On electric field penetration from ground into the ionosphere, J. Atmos. Solar-Terr. Phys., 341, 102-353.

Denisenko, V.V. (2015). Estimate for the strength of the electric field penetrating from the Earth's surface to the ionosphere, Russian J. Physical Chemistry, B9, N5, 789-795.

Freund, F., G. Ouillon, J. Scoville and D. Sornette (2021). Earthquake precursors in the light of peroxy defects theory: Critical review of systematic observations. Global Earthquake Forecasting System (GEFS) Special Issue: Towards using non-seismic precursors for the prediction of large earthquakes, Eur. Phys. Journal, 230, 7-46. https://doi.org/10.1140/epjst/e2020-000243-x

Gokhberg, M.B. and S.L. Shalimov (2000). Lithosphere-ionosphere coupling and their modelling, Russian J. Terrestrial Sciences, 2(2), 95-108.

Gousheva, M., D. Danov, P. Hristov and M. Matova (2008). Quasi-static electric fields phenomena in the ionosphere associated with pre- and post-earthquake effects, Nat. Hazards Earth Syst. Sci., 8, 101-107.

Grandshteyn, I.S. and I.M. Ryzhik (2007). Table of integrals, series and products, 7th edition, Elsevier Academic Press.

Hao, J., T.M. Tang and D.R. Li (2000). Progress in the research of atmospheric electric field anomaly as an index for short-impending prediction of earthquakes, J Earthquake Pred. Res., 8, 3, 241-255.

Harrison, R.G., K.L. Aplin and M.J. Rycroft (2010). Atmospheric electricity coupling between earthquake regions and the ionosphere, J .Atmospheric Solar-Terr. Phys., 72, 376-381.

Hayakawa, M., V.V. Surkov, Y. Fukumoto and N. Yonaiguchi (2007). Characteristics of VHF over-horizon signals possibly related to impending earthquakes and a mechanism of seismo-atmospheric perturbations, J. Atmos. Solar-Terr. Phys., 69, 1057-1062.

Hegai, V.V., V.P. Kim and J.Y. Liu (2015). On a possible seismomagnetic effect in the topside ionosphere, Adv. Space Res., 56, 1707-1713, http://dx.doi.org/10.1016/j.asr.2015.07.034

Jin, S., G. Occhipinti and R. Jin (2015). GNSS ionospheric seismology: Recent observation evidences and characteristics, Earth-Sci. Rev., 147, 54-64, https://doi.org/10.1016/j.earscirev.2015.05.003

Kamogawa, M. and Y. Kakinami (2013). Is an ionospheric electron enhancement preceding the 2011 Tohoku-Oki earthquake a precursor? J. Geophys. Res., 118, 1751-1754. https://doi.org/10.1002/jgra.50118

Kelley, M.C., W.E. Swartz and K. Heki (2017). Apparent ionospheric total electron content variations prior to major earthquakes due to electric fields created by tectonic stresses, J. Geophys. Res., 122, https://doi.org/10.1002/2016JA023601

Khegai, V.V. (2020). Analytical model of a seismogenic electric field according to data of measurements in the surface layer of the midlatitude atmosphere and calculation of its magnitude at the ionospheric level, Geomagn. Aeron., 60, 507-520, doi:10.1134/s0016793220030081

Kim, V.P., S.A. Pulinets and V.V. Hegai (2002). The theoretical model of the possible changes in the night-time midlatitude D-region of the ionosphere over the zone of strong earthquake preparation, Radiophys. Quantum Electron., 45, 289-296.

Kim, V.P., J.Y. Liu and V.V. Hegai (2012). Modeling the pre-earthquake electrostatic effect on the F region ionosphere, Adv. Space Res., 50, 1524-1533, http://dx.doi.org/10.1016/j.asr.2012.07.023

Kim, V.P., V.V. Hegai, J.Y. Liu, K. Ryu and J-K. Chung (2017). Time-varying seismogenic Coulomb electric fields as a probable source for pre-earthquake variation in the ionospheric F2-Layer, J. Astron. Space Sci., 34, 251-256, https://doi.org/10.5140/JASS.2017.34.4.251

Klimenko, M.V., V.V. Klimenko, I.E. Zakharenkova, S.A. Pulinets, B. Zhao and M.N. Tsidilina (2008). Formation mechanism of great positive TEC disturbances prior to Wenchuan earthquake on May 12, Advances Space Research, 48, N3, 488-499.

Korsunova, L.P. and V.V. Khegai (2018). Possible short-term precursors of strong crustal earthquakes in Japan based on data from the ground stations of vertical ionospheric sounding, Geomagn. Aeron., 58, 90-97.

Kuo, C.L., J.D. Huba, G. Joyce and L.C. Lee (2011). Ionosphere plasma bubbles and density variations induced by pre-earthquake rock currents and associated surface charges, J. Geophys. Res., 116, A10317. doi:10.1029/2011JA016628

Kuo, C.L., L.C. Lee and J.D. Huba (2014). An improved coupling model for the lithosphere-atmosphere-ionosphere system, J. Geophys. Res, 119, 3189-3205, doi:10.1002/2013JA019392

Le, H., L. Liu, J.Y. Liu, B. Zhao, Y. Chen and W. Wan (2013). The ionospheric anomalies prior to the M9.0 Tohoku-Oki earthquake, J. Asian Earth Science, 62, 476-484.

Liu, J.Y., Y.I. Chen, H.K. Jhuang, and Y.H. Lin (2004). Ionospheric foF2 and TEC anomalous days associated with M≥ 5.0 earthquakes in Taiwan during 1997-1999, Terr. Atmos. Oceanic Science, 15, 371-383.

Liu, J.Y. and C.K. Chao (2017). An observing system simulation experiment for FORMOSAT-5/AIP detecting seismo-ionospheric precursors, Terr. Atmos. Oceanic Sci, 28, 117-127, doi:10.3319/TAO.2016.07.18.01

Masci, F., J.N. Thomas and J.A. Secan (2017). On a reported effect in ionospheric TEC around the time of the 6 April 2009 L'Aquila earthquake, Nat Hazards Earth Syst Sci, 17, 1461-1468, doi:10.5194/nhess-17-1461-2017

Namgaladze, A.A. and M.I. Karpov (2015). Conduction current and extraneous electric current in the global electric circuit, Russ. J. Phys. Chem. B9, 754-757, https://doi.org/10.1134/S1990793115050231

Namgaladze, A., M. Karpov and M. Knyazeva (2018). Aerosols and seismo-ionosphere coupling: A review, J. Atmospheric and Solar-Terrestrial Physics, 171, 83-93.

Ouzounov, D., S. Pulinets, A. Romanov, K. Tsybulya, D. Davidenko, M. Kafatos and P. Taylor (2011). Atmosphere-ionosphere response to the M 9 Tohoku earthquake revealed by multi-instrument space-borne and ground observations: Preliminary results, Earthquake Science, 24, 557-564.

Park, C.G. and M. Dejnakarintra (1973). Penetration of thunderclouds electric fields into the ionosphere and magnetosphere, J. Geophys. Res., 78, 6623-6633.

Popov, L.N., Yu.K. Krakovezkiy, M.B. Gokhberg and V.A. Pilipenko (1989). Terrogenic effects in the ionosphere: a review, Phys. Earth Planet. Inter., 57, 115-128.

Prokhorov, B.E. and O.V. Zolotov (2017). Comments on "An improved coupling model for the lithosphere-atmosphere-ionosphere system" by Kuo et al. [2014], J. Geophys Res., 122, 4865-4868, doi:10.1002/2016JA023441

Pulinets, S.A., V.A. Alekseev, A.D. Legen'ka and V.V. Khegai (1997). Radon and metallic aerosols emanation before strong earthquakes and their role in atmosphere and ionosphere modification, Adv. Space Res., 20, 2173-2176.

Pulinets, S.A. and K.A. Boyarchuk (2004). Ionospheric precursors of earthquakes, Springer Verlag Publ.

Pulinets, S. and D. Ouzounov (2011) Lithosphere-atmosphere-ionosphere coupling (LAIC) model – An unified concept for earthquake precursors validation, J. Asian Earth Sci., 41, 371-382.

Pulinets, S. and D. Davidenko (2014). Ionospheric precursors of earthquakes and global electric circuit, Adv Space Res. 53, 709-723.

Pulinets, S.A., K.A. Boyarchuk, V.V. Hegai, V.P. Kim and A.M. Lomonosov (2000). Quasi-electrostatic model of atmosphere-thermosphere-ionosphere coupling, Adv. Space Res., 26, 1209-1218.

Rozhnoi, A.A., M.S. Solovieva, O.A. Molchanov, V. Chebrov, V. Voropaev, M. Hayakawa, S. Maekawa and P.F. Biagi (2006). Preseismic anomaly of LF signal on the wave path Japan-Kamchatka during November – December 2004, Phys Chem Earth, 31, 422-427.

Rulenko, O.P., A.V. Ivanov and A.V. Shumeiko (1992). Short-term atmospheric-electrical precursor to the Kamchatka earthquake of March 6, 1992, M = 6,1, Dokl. AN SSSR, 326, 980-982.

Rulenko, O.P. (2000). Operative precursors of earthquakes in the near-ground atmosphere electricity, Volcanol. Seismol., 4, 57-68.

Shalimov, S.L., A.A. Rozhnoy, M.S. Solov'eva and E.V. Ol'shanskaya (2019). Impact of earthquakes and tsunamis on the ionosphere, Phys. Solid Earth, 1, 199-213.

Sorokin, V.M., A.K. Yaschenko and M. Hayakawa (2007). A perturbation of DC electric field caused by light ion adhesion to aerosols during the growth in seismic-related atmospheric radioactivity, Nat. Hazards Earth Sys. Sci., 7, 155-163, doi:10.5194/nhess-7-155-2007

Sorokin, V. and M. Hayakawa (2013). Generation of seismic-related DC electric fields and lithosphere-atmosphere-ionosphere coupling, Modern Appl. Sci., 7, 6, doi:10.5539/mas.v7n6p1

Sorokin, V. and M. Hayakawa (2014). Plasma and electromagnetic effects caused by the seismic-related disturbances of electric current in the global circuit, Modern Appl. Sci., 8, 4, doi:5539/mas.v8n4p 61

Sorokin, V.M. and Yu.Ya. Ruzhin (2015). Electrodynamic model of atmospheric and ionospheric processes on the eve of an earthquake, Geomagn. Aeron., 55, 626-642, https://doi.org/10.1134/S0016793215050163

Sorokin, V.M., A.K. Yashchenko and V.V. Surkov (2019). Generation of geomagnetic disturbances in the ionosphere by a tsunami wave, Geomagn. Aeron., 59, 236-248, doi:10.1134/S001679401902013

Surkov, V.V. (2015). Pre-seismic variations of atmospheric radon activity as a possible reason for abnormal atmospheric effects, Annals Geophysics, 58, A0554, doi:10.4401/ag-6808

Surkov, V.V., V.A. Pilipenko and A.S. Silina (2022). Can radioactive emanations in a seismically active region affect atmospheric electricity and the ionosphere? Phys. of the Solid Earth, 58, 297-305, https://doi.org/10.1134/S1069351322030090

Thomas, J.N., J. Huard and F. Masci (2017). A statistical study of global ionospheric map total electron content changes prior to occurrences of M ⩾ 6.0 earthquakes during 2000-2014, J. Geophys. Res., 122, 2151-2161. https://doi.org/10.1002/2016JA023652

Virk, H.S. and B. Singh (1994). Radon recording of Uttarkashi earthquake, Geophys Res Lett, 21, 737-742.

Xu, T., H. Zhang, Y. Hua and J. Wu (2015). Electric field penetration into the ionosphere in the presence of anomalous radon emanation, Adv. Space Res., 55, 2883-2888 https://doi.org/10.1016/j.asr.2015.03.015

Yasuoka, Y., Y. Kawada, H. Nagahama, Y. Omori, T. Ishikawa, S. Tokonami and M. Shinogi (2009). Pre-seismic changes in atmospheric radon concentration and crustal strain, Phys. Chem. Earth, 34, 431-434.

Zolotov, O.V., A.A. Namgaladze, I.E. Zakharenkova, O.V. Martynenko and I.I. Shagimuratov (2012). Physical interpretation and mathematical simulation of ionospheric precursors of earthquakes at midlatitudes, Geomagn. Aeron., 52, 390-397.

***CORRESPONDING AUTHOR: Vyachelsav A. PILIPENKO**,
Institute of Physics of the Earth, Russian Academy of Sciences, B. Gruzinskaya 10, Moscow 123242, Russia
e-mail: space.soliton@gmail.com